# Chiral recognition between dissymmetric Tb- and Eu(pyridine-2,6-dicarboxylate)(3)(3-) complexes and Fe(III) proteins in aqueous solution. Luminescence quenching by cytochrome c from horse heart and cytochrome c-550 from Thiobacillus versutus and its Lys14- Glu and Lys99- Glu mutants

Meskers, S.C.J.; Ubbink, M.; Canters, G.W.; Dekkers, H.P.J.M.

# Chiral Recognition between Dissymmetric Tb- and Eu(pyridine-2,6-dicarboxylate)$_3^{3-}$ Complexes and Fe(III) Proteins in Aqueous Solution. Luminescence Quenching by Cytochrome *c* from Horse Heart and Cytochrome *c*-550 from *Thiobacillus versutus* and Its Lys14 → Glu and Lys99 → Glu Mutants

**Stefan C. J. Meskers, Marcellus Ubbink,† Gerard W. Canters, and Harry P. J. M. Dekkers***

*Gorlaeus Laboratories, Leiden Institute of Chemistry, Leiden University, NL-2300-RA Leiden, The Netherlands*

*Received: May 13, 1996; In Final Form: July 10, 1996*[⊗]

The enantioselective quenching of the luminescence of *racemic* Ln(DPA)$_3^{3-}$ (Ln = Tb, Eu; DPA = 2,6-pyridinedicarboxylate) by ferricytochrome *c* proteins in aqueous solution has been studied by time-resolved luminescence and circular-polarization-of-luminescence spectroscopy. All title proteins appear to be very efficient quenchers with quenching rate constants on the order of $10^7-10^9$ $M^{-1}$ $s^{-1}$ depending on the nature of the protein and Ln, on the absolute configuration of the Ln complex ($\Delta$ or $\Lambda$), and on the solution's ionic strength *I*. The ratio of the individual diastereomeric quenching rate constants, $k_q^{\Delta}/k_q^{\Lambda}$, ranges from 1.2 up to 3 depending on the nature of the protein and Ln ion, but hardly on *I*. The average quenching rate, $k_q^{av}$ ($=(k_q^{\Delta} + k_q^{\Lambda})/2$), also depends on the *ground state* lanthanide concentration, which allows for an estimate of the binding constant of ground state Ln complex to the active site of the protein: $7 \times 10^2$ (cytc) and $4 \times 10^2$ $M^{-1}$ (cytc-550) at $I = 0.022$ M. The quenching process is modeled by a two-step reaction pathway: (i) formation of an encounter complex between protein and excited Ln(DPA)$_3^{3-}$, at sites which are primarily determined by the electrostatic potential *V* around the protein molecules in the aqueous salt solutions, and (ii) transfer of electronic energy transfer from the excited Ln(DPA)$_3^{3-}$ to the heme chromophore. The potentials *V* calculated at positions near the exposed heme edge account qualitatively for the observed *I*-dependence of the quenching rates. The large enantioselectivities show that energy transfer takes place in conformations where the Ln complex and the protein are in intimate contact, and the large magnitude of $k_q^{av}$ shows that the contact takes place at the solvent exposed heme edge. While the enantioselectivities for the wild type and Lys14 → Glu cytc-550 are almost equal, that for the Lys99 → Glu mutant is considerably lower. This indicates that the quenching site is closer to Lys99 than to Lys14. Molecular modeling was used to optimize geometries of $\Delta$- and $\Lambda$-Ln(DPA)$_3^{3-}$/cytc-550 complexes in which a hydrogen bond between the $\epsilon$-amino group of Lys99 and the carboxyl group of a DPA ligand is present, yielding tentative structures of the diastereomeric complexes in which the energy transfer occurs.



## Introduction

The phenomenon of enantioselective quenching of luminescence has been studied intensively in recent years.[1−11] In these experiments a small quantity of enantiomerically resolved quencher, Q, is added to a solution containing a racemic mixture of luminescent molecules. If the chiral quencher discriminates between the two enantiomers of the luminophore, this is evidenced by a nonexponential luminescence decay curve and a nonvanishing degree of circular polarization of the luminescence. Tris terdentate Ln(III) (2,6 pyridinedicarboxylate = DPA)$_3^{3-}$ (Ln = Tb, Eu, Dy) complexes have been mostly used as luminophores; they have approximate $D_3$ symmetry and exist in two enantiomeric forms. On a laboratory time scale both forms are rapidly interconverting, and hence the solution is racemic (but at room temperature, the rate of racemization is slow compared to the excited state lifetime[12]). The chiral quenchers used were mainly tris-chelates such as tris(ethylenediamine)cobalt(III), tris(cyclohexanediamine)cobalt(III), and tris(phenantroline)ruthenium(II). The quenching has been ascribed to energy transfer from the luminophore to Q.

The proteins myoglobin,[13] transferrin,[14] and cytochrome *c*[15] have been reported to quench the luminescence of EDTA-type chelates of Tb(III) by energy transfer from the excited Tb complex to the ferriprotein. Enantioselectivity in such quenching reactions has, however, not reportedly been studied as yet. On the other hand, it is known that metalloproteins show, sometimes considerable, chiral discrimination in *electron* transfer reactions with optically active inorganic compounds.[16,17]

We decided to search for enantioselectivity in the energy transfer processes leading to quenching of the luminescence of Tb(DPA)$_3^{3-}$ and Eu(DPA)$_3^{3-}$ by metalloproteins. Among other things such effects might provide information on the stereochemical structure of these proteins, which may be complementary to that from electron transfer studies. In this paper we report the results obtained on some *c*-type ferricytochromes: mitochondrial cytc from horse heart muscle and bacterial cytc-550 from *Thiobacillus versutus*. Of this latter protein (wild type, wt), we also studied two mutants: one with lysine 14 replaced by a glutamate (K14E) and the other with lysine 99 replaced (K99E).

## Theory

**Introduction.** The overall luminescence quenching reaction is given by (1), where $\sigma$ stands for $\Delta$ or $\Lambda$, i.e., the two enantiomers present in a racemic solution of Ln(DPA)$_3^{3-}$, which we will abbreviate as Ln. The lanthanide complexes in the

* Author to whom correspondence should be addressed at: Gorlaeus Laboratories, Leiden Institute of Chemistry, Leiden University, P.O. Box 9502, NL-2300-RA Leiden, The Netherlands. Telephone: +31 71 5274263. Fax: +31 71 5274488. E-mail: Dekkers@chem.leidenuniv.nl.

† Present address: Department of Biochemistry, University of Cambridge, U.K.

⊗ Abstract published in *Advance ACS Abstracts,* October 15, 1996.

S0022-3654(96)01381-0 CCC: $12.00 

excited state are denoted by Ln*. Q denotes the chiral quencher molecule and Q* denotes an electronically excited state of Q.

$$\sigma\text{-Ln}^* + \text{Q} \rightarrow \sigma\text{-Ln} + \text{Q}^* \quad (1)$$

Upon excitation with *unpolarized* light the excited state population is racemic. The Δ-Ln* and Λ-Ln* species can return to the ground state by spontaneous emission (luminescence) and by nonradiative decay. The total decay rate, $k_0$, is equal for both enantiomers in the absence of Q. In the presence of quencher an extra decay channel is opened with a rate which equals the product of the molar quenching rate constant $k_q$ and the quencher concentration; see (2). This equation allows for enantioselectivity because the rate constants for the quenching of Λ- and Δ-Ln* by the chiral protein may differ: $k_q^{\Lambda} \neq k_q^{\Delta}$.

$$k^{\sigma} = k_0 + k_q^{\sigma}[\text{Q}] \quad (2)$$

The information on the enantioselectivity of the quenching reaction is contained in the pair of diastereomeric rate constants $k_q^{\Delta}$ and $k_q^{\Lambda}$. Alternatively, it is carried by the quantity $E_q$ in (3), which is defined in analogy to the concept enantiomeric excess in synthetic chemistry, along with the average quenching rate constant $k_q^{av}$ of (4).

$$E_q = (k_q^{\Delta} - k_q^{\Lambda})/(k_q^{\Delta} + k_q^{\Lambda}) \quad (3)$$

$$k_q^{av} = (1/2)(k_q^{\Delta} + k_q^{\Lambda}) \quad (4)$$

**Measurement of the Enantioselectivity.** In view of (2), the decay of the Ln* emission, $I(t)$, after a short pulse of unpolarized excitation light is represented by (5). It has been shown[8] that fitting the luminescence decay data to the four-parameter function, (6), in which $d$ takes into account the dark current of the light detector, yields accurate values of $|E_q|$, provided this quantity is not too small (0.06 for the typical sampling times used in the present study). Measurement and analysis of the luminescence decay offer a quick route toward $|E_q|$ data because the entire emission spectrum can be used as a probe. Although two diastereomeric quenching rate constants are obtained, one needs a chirooptical experiment to assign $k_q^{\Lambda}$ to one and $k_q^{\Delta}$ to the other.

$$I(t) = A\{\exp(-k^{\Delta}t) + \exp(-k^{\Lambda}t)\} \quad (5)$$

$$I(t) = A(\exp(-bt) + \exp(-ct)) + \text{d} \quad (6)$$

Circular polarization of the luminescence (CPL), the emission analogue of circular dichroism, results from the luminescence of a pure enantiomer containing unequal amounts of left ($I_L$) and right circularly polarized light ($I_R$). The sign of the dissymmetry factor, $g_{lum}$, for a given electronic transition, (7), is positive for one enantiomer and negative for the other. If this correlation is known, as is the case for the luminophores we use in this study, from the *sign* of the CPL in the quenching experiment, one can determine which enantiomer is preferentially quenched and thus assign the slower and faster quenching rate constant to $k_q^{\Lambda}$ and $k_q^{\Delta}$.

$$g_{lum} = 2(I_L - I_R)/(I_L + I_R) \quad (7)$$

Time-resolved (TR) or steady-state CPL measurements also provide quantitative results on the quenching processes. With continuous wave (cw) excitation the degree of circular polarization in the luminescence is equal to (8) which can be rewritten as (9). Therefore, the magnitude and the sign of $E_q$

$$g_{lum}^{cw}(\lambda) = g_{lum}^{\Lambda}(\lambda)\,(k_q^{\Delta} - k_q^{\Lambda})[\text{Q}]/(2k_0 + (k_q^{\Delta} + k_q^{\Lambda})[\text{Q}]) \quad (8)$$

$$E_q = \{g_{lum}^{cw}(\lambda)/g_{lum}^{\Lambda}(\lambda)\}\{(k_q^{av}[\text{Q}] + k_0)/k_q^{av}[\text{Q}]\} \quad (9)$$

can be established from $g_{lum}^{cw}(\lambda)$ provided that $k_q^{av}$ and the constants $g_{lum}^{\Lambda}(\lambda)$ and $k_0$ are known. Values for $k_q^{av}$ and $k_0$ can be found from the luminescence decay and the value of $g_{lum}^{\Lambda}(\lambda)$ from a TR-CPL measurement. While $|E_q|$ can be determined from decay analysis, the measurement of the circular polarization provides another essentially independent method for finding $E_q$.

In a TR-CPL experiment one utilizes pulsed excitation light, and $g_{lum}$ is measured as a function of the time after the pulse; see (10). The equation predicts that $g_{lum}(\lambda,t)$ is zero at $t = 0$ and increases with time to the asymptotic value $g_{lum}^{\Lambda}(\lambda)$—if the Λ-enantiomer is quenched slower. By fitting a tanh function to the TR-CPL signal, the values of $g_{lum}^{\Lambda}(\lambda)$ and $(k_q^{\Delta} - k_q^{\Lambda})$ can be determined, and by dividing the latter by $2k_q^{av}$, the value of $E_q$ can be obtained.

$$g_{lum}(\lambda,t) = g_{lum}^{\Lambda}(\lambda)\,\tanh\{(1/2)(k_q^{\Delta} - k_q^{\Lambda})[\text{Q}]t\} \quad (10)$$

**Model of the Quenching Reaction.** We model the bimolecular quenching reaction in (1) as follows; see Scheme 1. A very small fraction of the Ln ions is photoexcited by irradiation in a ligand absorption band, and they very quickly relax to the luminescent state. These Ln* species and the quencher molecule Q have to diffuse together (rate constant $k_d$) to form a reactive encounter complex {Ln*Q}. This complex may dissociate again ($k_{-d}$) or undergo the actual quenching reaction which we assume to be a short-range (nonradiative) electronic energy transfer to Q (rate constant $k_{et}$). We will neglect back energy transfer because the complex {LnQ*} has a very short lifetime (ferricytochrome *c* species are nonfluorescent at room temperature). The quantities $k_0$ and $k_0'$ denote the rate constants of luminescent decay of free and bound Ln*; $k_0'$ is expected to be of the same order of magnitude as $k_0$ ($10^3$ $s^{-1}$ for Ln = Tb, Eu). We include in the scheme the formation ($k_d'$) and dissociation ($k_{-d}'$) of ground state encounter complexes {LnQ}; the associated equilibrium constant is denoted by $K'$.

**SCHEME 1**

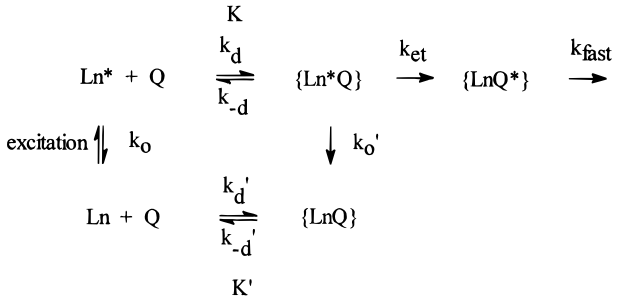


In our experiments we use samples where [Ln] is typically $\sim 10^{-3}$ M and [Q] is $\sim 10^{-5}$ M, which has several implications. (i) Direct excitation of Ln in {LnQ} can be neglected. Even if every quencher molecule is bound to an Ln ion the ratio [{Ln*Q}]/[Ln*] is only 1%. (ii) A quencher concentration of $10^{-5}$ justifies the steady-state approximation for {Ln*Q}: $k_d[\text{Q}] \ll k_{-d} + k_{et} + k_0'$. This is because $k_d/k_{-d}$, which by definition equals the pseudo equilibrium constant $K$ for encounter complex formation, certainly is smaller than $1/[\text{Q}] = 10^5$. (iii) The excess

of Ln can (and does) lead to a substantial fraction of Q being bound to (ground state) Ln. As compared to Q, {LnQ} will be a much more ineffective quencher for the triply charged Ln* anion than Q (because of the extra −3 charge). Consequently this results in a lowering of effective quencher concentration.

For such samples the complete time dependence of the [Ln*] species, and thus of the Ln* emission intensity, after the excitation pulse can be calculated,[6,18] which eventually leads to (11). The same kinetic equation is obtained directly when adopting the steady-state approximation for {Ln*Q}:

$$k = k_0 + \frac{k_d k_{et}}{k_{-d} + k_{et}}[Q] = k_0 + k_q[Q] \qquad (11)$$

In the denominator of (11) the term $k_0'$ has been neglected. If we assume that the quenching reactions are not substantially diffusion influenced (for which we have evidence—although not conclusive; see Discussion section), i.e., that $k_{et} \ll k_{-d}$, $k_q$ is given by the right hand side of (12). In (12) we have reattached the $\sigma$-label which accounts for the fact that the rate constants $k_{-d}$ and $k_{et}$ may be different for the two diastereomeric systems. One expects, however, that chiral discrimination in $k_d$ is small since a large part of the diffusional trajectory involves large Ln−Q separations in the (achiral) solvent.[9,10]

$$\frac{1}{k_q^{\sigma}} = \frac{1}{k_d^{\sigma}} + \frac{1}{K^{\sigma} k_{et}^{\sigma}} \cong \frac{1}{K^{\sigma} k_{et}^{\sigma}} \qquad (12)$$

In the case that the quenching does not take place at a single intermolecular configuration, (12) can be generalized. If $(R,\alpha)$ denotes a set of coordinates describing the relative position and orientation of the donor and quencher molecule, we have

$$k_q^{\sigma} = \int g^{\sigma}(R,\alpha) k_{et}^{\sigma}(R,\alpha)\, dR\, d\alpha = \int \exp(-w^{\sigma}(R,\alpha)/k_B T)\, k_{et}^{\sigma}(R,\alpha)\, dR\, d\alpha \qquad (13)$$

where $g^{\sigma}(R,\alpha)$ is a distribution function. The product $[\sigma\text{-Ln*}]\text{-}g^{\sigma}(R,\alpha)$ gives the local concentration, at position $R$, of $\sigma$-Ln* complexes with specified orientation relative to a (free) quencher molecule at $R = 0$. The right-hand side of (13) arises because formally $g^{\sigma}(R,\alpha)$ can be written as $\exp(-w^{\sigma}(R,\alpha)/k_B T)$ where $w^{\sigma}(R,\alpha)$ denotes the potential of mean force between the donor and quencher.[19]

## Materials and Methods

**Purification of the Proteins.** cytc (Sigma Chemicals) was dissolved in 10 mM phosphate buffer (pH 7.6), and a small amount of potassium ferricyanide was added to ensure that all protein molecules are in the ferric state. FPLC (Pharmacia L.K.B.) was employed to purify the protein. Column material was Sepharose S (column dimensions 15 × 2.6 cm), and the salt gradient was 0−200 mM NaCl. The relevant fractions were desalted and concentrated with an Amicon stirred cell with Amicon YM10 membrane. The isolation and purification of the cytc 550 proteins from *T. versutus* were performed as described elsewhere: wt cytc-550,[20,21] K14E cytc-550,[22] and K99E.[23]

**Preparation of Samples.** The $Ln(DPA)_3^{3-}$ complexes were prepared as described earlier.[8] In the spectroscopic samples, [Ln] normally was taken to be ∼1 mM but in some experiments a lower concentration was chosen; see text. Protein concentrations were determined spectrophotometrically, using as values of the extinction coefficients at 550 nm $8.4 \times 10^3$ $M^{-1}$ $cm^{-1}$ [24] and $10.3 \times 10^3$ $M^{-1}$ $cm^{-1}$ [20] for oxidized cytc and oxidized cytc-550, respectively.

**Measurements.** The time-resolved luminescence measurements and the TR and cw CPL experiments were performed on a custom-designed photon-counting instrument,[25] which for this work was equipped with a cooled (−30 °C) red-sensitive photomultiplier tube (Hamamatsu, R1463-01). In the TR experiments a pulsed xenon lamp (Optitron, NR 1B) was used as the excitation source, and in the steady-state experiments a 900 W xenon arc lamp was used. Excitation-wavelength selection was done with a monochromator (Minimate, Spex) and/or optical filters. Absorbance measurements were made on a Perkin Elmer Lambda 6 spectrophotometer, and pH values were determined with a digital pH meter (Consort). Luminescence decay and TR-CPL curves were analyzed by a nonlinear least-squares curve-fitting procedure based on the Levenberg−Marquardt algorithm[26] as described previously.[8] Unless otherwise specified, all measurements were performed at room temperature (20 ± 1 °C). Preliminary measurements showed only a small temperature dependence of the quenching rate constants (activation energies ∼1 kcal/mol).

**Electrostatic Potentials.** Use was made of the molecular structure of horse heart cytc as determined by Qi et al.[27] Coordinates (entry 1FRC version July 30 from PDB) were obtained from the Protein Data Bank[28,29] at Brookhaven National Laboratory. In the model the charged amino acid side chains are to be represented by point charges. We assume[15,30] that all Asp, Glu side chains as well as the heme propionates and the terminal carboxyl group are negatively charged. The charge was positioned at a single O atom of the carboxyl group proteins. The Arg and Lys side chains are represented by a +1 unit charge on respectively the $N_{\eta 1}$ and $N_\zeta$ atom, His by a $+^1/_2$ charge on $N_\epsilon$ (except His18 which is coordinated to Fe), and the porphyrin ring by a +1 charge at the Fe atom.[15,30] For some charges the distance to the center had to be decreased slightly to bring them inside or on the surface of a sphere around the center of mass with a radius of 20 Å for cytc and 21 Å for cytc-550. These numbers are 1 Å smaller than the adopted radii of the dielectric boundary between the inside of the protein ($\epsilon_1 = 2$) and the solvent (water-containing salt, $\epsilon_2$ taken as 78.5). For the maps in Figure 7, $V$ was calculated for different values of $\theta$, $\phi$ keeping $R$ constant. For cytc $R = 25$ Å was chosen (26 Å for cytc-550), i.e., the radius of the dielectric boundary plus 4 Å as an estimate of the van der Waals radius of the $Ln(DPA)_3^{3-}$ complexes. In the calculations we have truncated the multipole expansion of $V$ after the 10th moment as at this point convergence always had occurred. To evaluate $k_q$, $V$ values at larger $R$ were calculated as well.

For cytc-550 we have used the coordinates (entry 1COT, version Sept 3, 1994) of cyt-$c_2$ (earlier referred to as cytc-550) from *Paracoccus denitrificans*[31] (Pd). These two proteins are highly homologous, but some of the charged amino acid residues are different, which was taken into account as follows. In the model of *T. versutus* cytc-550 (Tv) the charge representing Glu2 was positioned at the $C_\alpha$ atom of the Asp2 residue in Pd (the Asp2 side chain is not resolved), the Tv Asp57 charge was positioned at the $O_{\epsilon 2}$ atom of Glu57 in Pd, Tv Glu 89 at the $N_\zeta$ atom of Pd Lys 89, Tv Lys 90 at the S atom of Pd Met 90, and Tv His 118 at the $N_{\delta 1}$ atom of Pd Asp121. It is known that the C terminal region of the Tv c550 protein is sensitive to cleavage.[21] Therefore, the charged amino acid residues Glu125 and Glu131 were not taken into account, and the terminal carboxyl group was positioned at the Ala122 residue in the Pd structure. The N terminus was included as a +1 charge on the N atom. The position of this atom was taken from an older

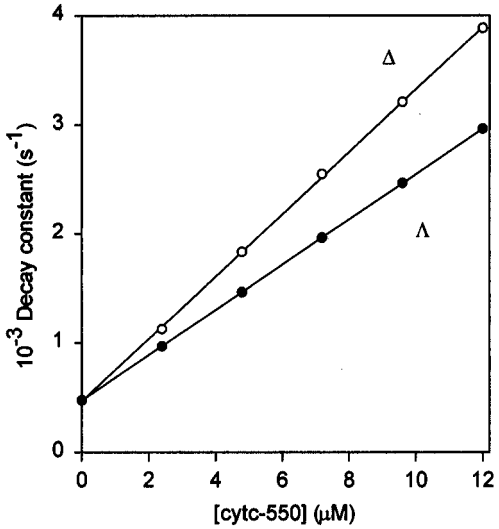


**Figure 1.** Stern−Volmer plots for the quenching of Λ,Δ-Tb(DPA)$_3^{3-}$ luminescence by cytc-550. The lines represent linear least-squares fits to the measured luminescence decay constants *k*. The upper line is assigned to Δ-Tb, the lower to Λ-Tb; see text. Experimental conditions: [Tb] = 1.0 mM, pH 7.2, Tris buffer 0.010 M, $I$ = 0.022 M.

**TABLE 1: Rate Constants and $E_q$ Values for Quenching of Tb(DPA)$_3^{3-}$ and Eu(DPA)$_3^{3-}$ Luminescence by Ferricytochromes**[a]

| | $k_q^{\Delta} \times 10^{-7}$ ($M^{-1}$ $s^{-1}$) | $k_q^{\Lambda} \times 10^{-7}$ ($M^{-1}$ $s^{-1}$) | $E_q$ (decay) | $E_q$ (glum$^{cw}$) |
|---|---|---|---|---|
| | | Tb(DPA)$_3^{3-}$ | | |
| cytc | 19 | 11 | +0.27±0.01 | +0.27±0.01 |
| cytc550 wt | 25 | 18 | +0.17±0.01 | +0.18±0.01 |
| K14E | 8.9 | 6.0 | +0.19±0.01 | +0.19±0.01 |
| K99E | 6.1 | 5.3 | +0.07±0.01 | +0.08±0.02 |
| | | Eu(DPA)$_3^{3-}$ | | |
| cytc | 11 | 4.0 | +0.47±0.01 | +0.50±0.01 |
| cytc550 wt | 9.1 | 6.1 | +0.20±0.01 | +0.20±0.01 |
| K14E | 2.8 | 1.8 | +0.22±0.02 | +0.23±0.01 |
| K99E | 1.9 | 1.5 | +0.10±0.02 | +0.10±0.01 |

[a] [Ln] = 1.0 mM; $I$ = 0.022 M; 10 mM Tris, pH = 7.2. Standard error in the rate constants is ~1 × $10^7$ ($M^{-1}$ $s^{-1}$), standard error in $E_q$ is given in the table. Values of $k_q$ are obtained using the total quencher concentration. When the lower effective [Q] is taken into account, they should be multiplied by 1.7 (cytc) and 1.4 (cytc-550).

crystal structure[32] (entry 155C version Oct 15, 1991 of PDB). In horse heart cytc the N terminus is acylated, and so it was not taken into account.

## Experimental Results

When small amounts of Fe(III)cytc-550 are added to a 1 mM aqueous solution of Tb(DPA)$_3^{3-}$, quenching of the lanthanide emission is readily observed: the intensity and lifetime of the emission decrease (but its spectral shape remains unchanged). The effect of quencher concentration on the decay constants is shown in Figure 1. At each protein concentration investigated, the values of the two decay constants have been extracted by fitting (6) to the observed emission decay. From this Stern−Volmer plot, the two molar quenching constants $k_q^{\Delta}$ and $k_q^{\Lambda}$ are found, and these clearly are different. Using (2), (3), and $k_0$(Tb) = 472 $s^{-1}$, $|E_q|$ is found to be 0.17. Also in the case of cytc as the quencher, we observe linear Stern−Volmer plots. The values for $k_q^{\Delta}$, $k_q^{\Lambda}$, and $E_q$ are collected in Table 1.

While the biexponential decay of the luminescence suggests enantioselectivity in the quenching, optical activity provides proof. Figure 2 shows the total intensity, $(I_L + I_R)/2$, and the differential intensity, $(I_L - I_R)$, of the $^7F_5 \leftarrow {}^5D_4$ emission of

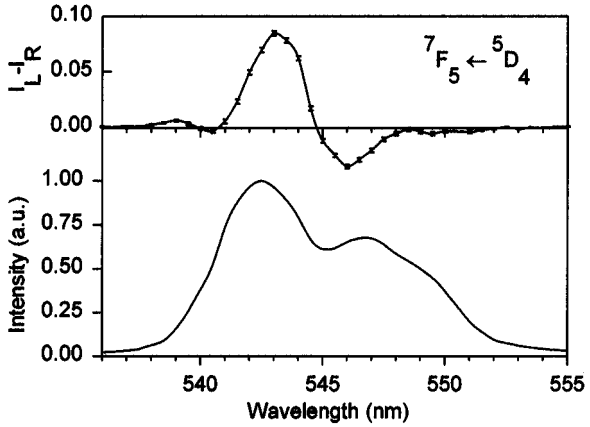


**Figure 2.** Total intensity (bottom) and circular intensity differential (top) of Tb $^7F_5 \leftarrow {}^5D_4$ emission in the presence of cytc. Experimental conditions: [Tb] = 1.0 mM, [cytc] = 11 μM, $I$ = 0.012 M, unbuffered solution, pH ~ 7, spectral resolution 1 nm. The vertical bars represent standard errors.

Tb* in the system Tb/cytc; their shapes are identical to those reported earlier.[33] Since the value of $g_{lum}$ for the 543 nm emission band of the Λ-enantiomer of Tb(DPA)$_3^{3-}$, $g_{lum}^{\Lambda}$(543 nm), is positive,[8] it follows that there is an excess of Λ-Tb* in the excited state implying that the Δ-enantiomer of Tb* is quenched faster by cytc than the Λ-form. Also in the quenching by the wild type cytc-550 and its K14E and K99E mutants, a positive circular polarization of the residual Tb* emission at 543 nm is observed, and hence all proteins studied show a preference for Δ-Tb* in the energy transfer. A similar conclusion holds for Eu (the relevant value of $g_{lum}^{\Lambda}$(595 nm) is positive as well[8]).

Definite proof that the observed enantioselective quenching effects are of dynamic nature is provided by the time-resolved CPL data. In Figure 3 we depict the time dependence of $g_{lum}$ in the strong Tb* $^7F_5 \leftarrow {}^5D_4$ transition at $\lambda$ = 543 nm in the presence of cytc. It appears to be zero right after the excitation pulse which shows that there is no enantiomeric enrichment of Tb* at $t$ = 0, so the observed chiral discriminations cannot be due to ground state associations (e.g., Pfeiffer effect). The figure nicely demonstrates that the degree of circular polarization approaches a plateau value in the tail of the luminescence decay curve (where emission intensity is very small and, thus, noise in the $g_{lum}$ data very high). From fitting the tanh function from (10) to the data, the optimum parameters are found to be $g_{lum}^{\Lambda}$(543 nm) = +0.30 ± 0.01 (standard error) and $(k^{\Delta} - k^{\Lambda})$ = 1948 ± 54 $s^{-1}$. The weighted residuals and their autocorrelation function illustrate the quality of the fit. The resulting value of $E_q$, +0.31 ± 0.01, compares well with that obtained from the decay analysis (+0.29 ± 0.01). We also find that the intensity-weighted time average of the $g_{lum}(t)$ signal is, within experimental error, equal to the observed value of $g_{lum}^{cw}$. Use of (9) and the experimental values for $g_{lum}^{\Lambda}$ and $k_q^{av}$ yields the value +0.31 ± 0.01 for $E_q$.

The enantioselectivity in the quenching of Eu* by cytc appears to be higher than that of Tb. From a fit of the $g_{lum}(t)$ data measured in the $^7F_1 \leftarrow {}^5D_0$ band (see Figure 3) we find $g_{lum}^{\Lambda}$(595 nm) = +0.43 ± 0.013 and $(k^{\Delta} - k^{\Lambda})$ = 1435 ± 72 $s^{-1}$. Along with the value of $k_q^{av}$, the latter number implies that $E_q$ amounts to +0.51 ± 0.025 (decay analysis using $k_0$(Eu) = 622 $s^{-1}$: +0.50 ± 0.01). Again the time average of the $g_{lum}(t)$ signal equals the directly measured $g_{lum}^{cw}$. From cw-CPL the value of $E_q$ is found to be +0.51 ± 0.01 when the experimental value for $k_q^{av}$ is used together with $g_{lum}^{\Lambda}$ ($\lambda$ = 595 nm) = +0.45, the latter value resulting from a separate, dedicated experiment (inset, Figure 3).

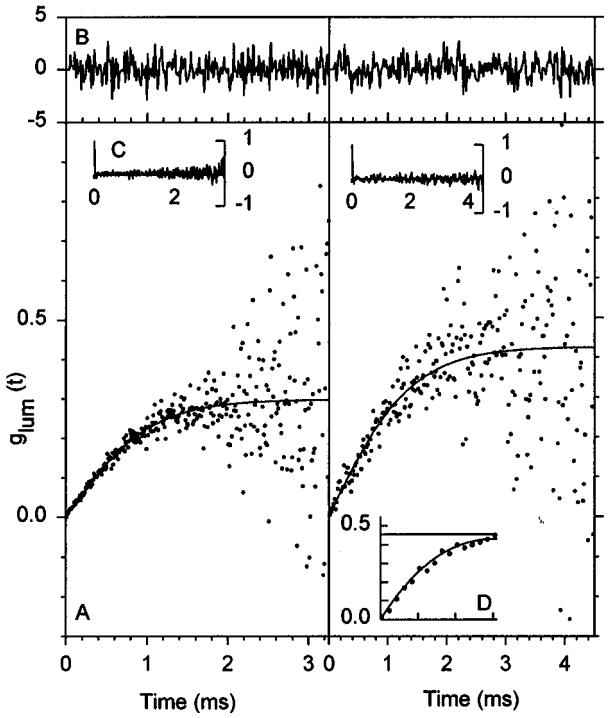


**Figure 3.** Time dependence of the degree of circular polarization, $g_{lum}$, of the strong Tb $^7F_5 \leftarrow {}^5D_4$ transition at 543 nm of Tb/cytc (left) and of the Eu $^7F_1 \leftarrow {}^5D_0$ transition at 595 nm of Eu/cytc (right). (A) Data points observed. The time axis displayed corresponds to 512 time channels and equals more than 10 times the excited state life time. The solid line is the result of a two-parameter fit of (10). The weighted residuals from the tanh fit are given in (B), the autocorrelation function of the weighted residuals in (C). The insert (D) displays the $g_{lum}(t)$ curve obtained from a separate measurement of Eu/cytc in unbuffered $D_2O$ at the same wavelength and band pass settings. Experimental conditions for Tb/cytc: [Tb] = 1mM, [cytc] = 12$\mu$M, unbuffered solution, $I$ = 0.012 M, spectral bandwidth 2 nm. Same for Eu/cytc except for the spectral resolution (4 nm).

With cytc-550 as the quencher, the TR-CPL data show zero activity at $t = 0$ and an increase thereafter, but, due to lower enantioselectivity, $g_{lum}(t)$ does not reach a clear plateau value. However, also for this system the values of $E_q$ as found from analysis of the emission decay and the time-resolved CPL signal appear to be equal.

In Table 1 we summarize the results for the quenching of Tb* and Eu* by cytc, wild type cytc-550, and the K14E and K99E mutants in buffered solution. Given are the rate constants of quenching of the $\Lambda$- and $\Delta$-luminophores, the values of $E_q$ obtained from the decay analysis, and those from $g_{lum}{}^{cw}$ measurements. In calculating the latter $E_q$ data we have used the following values of $g_{lum}{}^{\Lambda}$: +0.30 ($\Lambda$-Tb, $\lambda$ 543 nm, bandwidth 2 nm) and +0.45 ($\Lambda$-Eu; $\lambda$ = 595 nm, 4 nm). It emerges that the value of $E_q$ pertaining to the Tb/cytc system in a buffered system ($E_q = 0.27 \pm 0.01$, Table 1) is somewhat smaller than that in the unbuffered solution mentioned above, but the difference is close to the experimental error.

Very interesting from a spectroscopic point of view is the fact that the value of $g_{lum}{}^{\Lambda}$ of the Eu emission at 595 nm is considerably higher than reported previously.[4,34] As yet we have no explanation for this.

**Effects of I and [Ln]**. Upon addition of NaBr to a sample containing 1 mM Tb, 10 mM Tris buffer, pH 7.2, and 11 $\mu$M cyt-c550, a solution having an intrinsic ionic strength of 0.022 M, a decrease of the rate of quenching is observed, which indicates that there is a attractive interaction between the Ln species (with charge $q_{Ln} = -3|e|$) and the quenching site of the negatively charged protein. Figure 4 shows that in the region

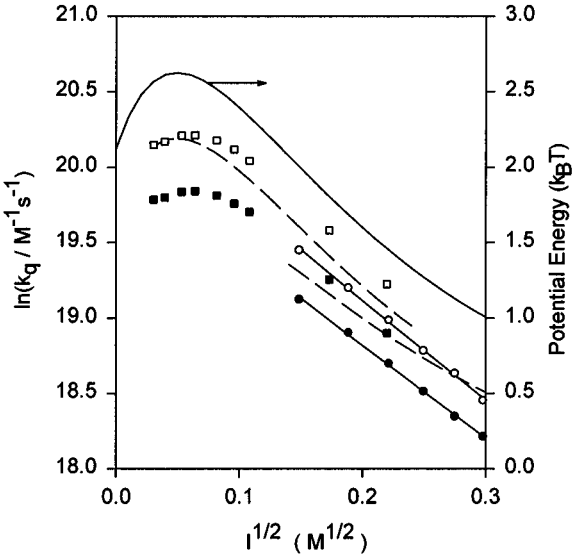


**Figure 4.** Effect of ionic strength on the quenching rate constants of Tb/cytc-550. The circles represent the data points pertaining to a sample with [Tb] = 1.0 mM, [cytc-550] = 11 $\mu$M, 10 mM Tris buffer, and pH 7.2 (initial ionic strength 0.022 M) to which NaBr is added. The solid straight lines are fits to these data points. The square data points are obtained with a dilute unbuffered solution of 0.1 mM Tb and 11 $\mu$M cytc-550 to which NaBr is added. The full curve shows the electrostatic potential energy calculated for the donor/acceptor system. The broken lines represent the predicted $I$-dependence of the average quenching rate making use of the calculated potential energies and of (19) and (20); the upper curve pertains to [Tb] = 1.0 mM, the lower one to [Tb] = 0.1 mM. Open symbols pertain to $\Delta$-Tb, filled symbols to $\Lambda$-Tb.

**TABLE 2: Salt Effect on the Quenching Rate Constants**[a]

| | ln($k_q^{\Delta}$) at $I = 0$ | slope ($M^{-1/2}$) | ln($k_q^{\Lambda}$) at $I = 0$ | slope ($M^{-1/2}$) |
|---|---|---|---|---|
| | | $Tb(DPA)_3{}^{3-}$ | | |
| cytc | 20.3 | −7.6 | 19.8 | −7.4 |
| cytc[b] | 21.7 | −12.9 | 21.2 | −12.7 |
| cytc550 wt | 18.9 | −6.4 | 20.0 | −6.0 |
| K14E | 18.4 | −3.5 | 18.4 | −3.0 |
| K99E | 18.4 | −3.5 | 18.4 | −3.5 |
| | | $Eu(DPA)_3{}^{3-}$ | | |
| cytc | 19.8 | −8.3 | 18.7 | −8.3 |
| cytc-550 wt | 19.3 | −6.4 | 18.9 | −6.2 |
| K14E | 17.3[c] | −3.2[c] | 17.3[c] | −3.2[c] |
| K99E | 17.0[c] | −3.2[c] | 17.0[c] | −3.2[c] |

[a] Intercepts and slopes from linear least-squares fits of ln($k_q$/$M^{-1}$ $s^{-1}$) *vs* $I^{1/2}$; [Ln] = 1.0 mM. Estimated standard error in the intercepts $\pm$0.1, in the slopes $\pm$0.2. [b] Pertains to samples with [$Tb(DPA)_3{}^{3-}$] = 0.1 mM. [c] Only the average quenching rate constant, ($k_q^{\Delta} + k_q^{\Lambda}$)/2, could be determined.

$0.15 < I^{1/2} < 0.3$ $M^{1/2}$ the logarithms of the quenching rate constants decrease linearly with $I^{1/2}$; the intercepts and slopes are collected in Table 2. To study the low ionic strength region, we started out from a dilute, unbuffered solution of 0.1 mM Tb and 11 $\mu$M cytc-550 to which we added NaBr. Again, in the region $0.15 < I^{1/2} < 0.3$ $M^{1/2}$, the decrease of ln $k_q^{\Delta}$ (ln $k_q^{\Lambda}$) is proportional to $I^{1/2}$ with about the same slope as with the more concentrated solution, but with a different value of the intercept (Figure 4). This shows that for two samples with equal ionic strength, lower $k_q$ values are measured for the sample with the higher Ln concentration (see Discussion).

Analogous results for the quenching of Tb luminescence by cytc are given in Figure 5. Again the plots of ln $k_q^{\Delta}$ and ln $k_q^{\Lambda}$ *vs* $I^{1/2}$ are linear in the high $I$-region; slopes and intercepts are given in Table 2. As compared to cytc-550, a stronger $I$-dependence and a larger value of $K'$ are found (see below),

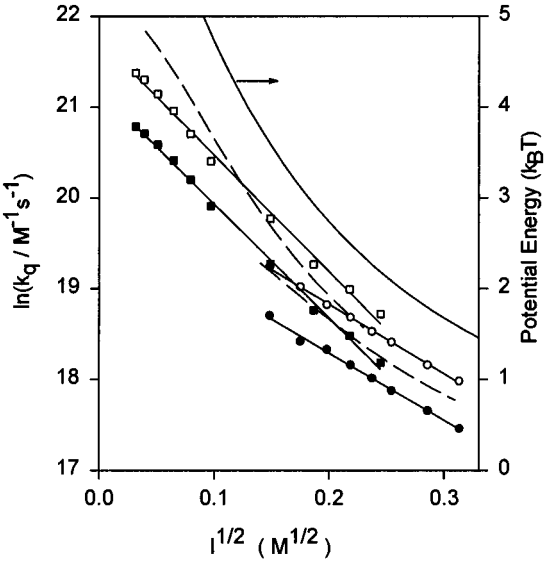


**Figure 5.** Effect of ionic strength on the quenching rate constants of the system Tb/cytc. See legend of Figure 4, except for protein concentration (∼12 $\mu$M).

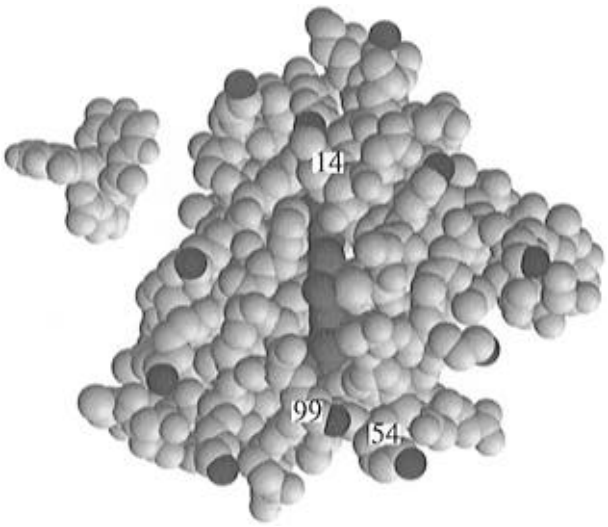


**Figure 6.** Structure of cytc-550 and Λ-Eu(DPA)$_3^{3-}$. A model of cytc-550 (based upon the structure of *P. denitrificans* cyt-c$_2$[31]). Grey: heme group, viewed edge on. Black: N$_\zeta$ atoms of the lysine residues. Hydrogen atoms of the protein are not shown. Upper left corner: Λ-Eu(DPA)$_3^{3-}$.

indicating that the positive charge on the cytc protein is larger. Interestingly, in the region $0.05 < I^{1/2} < 0.15$ M$^{1/2}$, the quenching rates for cytc increase monotonously upon lowering $I$, while the quenching rates for cytc-550 level off at $I^{1/2} = 0.08$ M$^{1/2}$ and even decrease slightly for $I^{1/2} < 0.08$ M$^{1/2}$. In the Discussion section we will propose an explanation for this peculiar behavior. For the cytc-550 mutants we have measured the $I$-dependence of the quenching rates in the range $0.15 < I^{1/2} < 0.33$ M$^{1/2}$ at one lanthanide concentration only. For both mutants ln $k_q^\sigma$ varies linearly with $I^{1/2}$; slopes and intercepts are listed in Table 2.

**Calculation of the Electrostatic Potential around the Proteins.** Cytc and cytc-550 are type I cytochrome *c* proteins[35,36] which have as a characteristic that part of the heme ring sticks out of the "heme pocket" and is exposed to the solvent. The exposed heme edge is surrounded by a ring of positively charged lysine residues (see Figure 6). While structurally similar, both protein molecules have very different charges: cytc has the isoelectric point, pI, at 10.0[37] and is therefore expected to have a large positive overall charge, while cytc-550 has pI 4.6[20] and thus has a net negative charge at pH ≈ 7. If net charges determined the effects,[38] the $k_q$ values of cytc would be much larger than for cytc-550, and their $I$-dependence would be in opposite directions, which is clearly not the case (see Tables 1 and 2). This suggests that the magnitude of the binding constant and its $I$-dependence are determined by the local charge near a specific energy transfer site.

To get an idea about the electrostatic potential $V$ around the proteins with their complex charge distributions, we have used the computationally fast approach derived by Head-Gordon and Brooks.[39] The authors provide an analytical expression for the potential due to an arbitrary distribution of point charges inside a sphere having radius $R_1$ and dielectric constant $\epsilon_1$, where the interior of the sphere represents the hydrophobic interior of a globular protein and the point charges represent the ionized residues of the protein. The sphere is impermeable for the ions from the surrounding aqueous electrolyte solution having dielectric constant $\epsilon_2$ and ionic strength $I$. For this system the linearized Poisson−Boltzmann equation can be solved yielding a multipole expression for the potential.

Figure 7A shows for equine cytc the calculated electrostatic potential energy ($=q_{Ln}V$) as a function of the latitude $\theta$ and the longitude $\phi$ of the 3$^-$ Ln species on the protein surface in units $k_BT$ at 293 K. In drawing the figure we have oriented the protein such that the line joining the N$_\zeta$-atoms of Lys13 and Lys79 has $\phi = 180°$ and the average position $\theta = 90°$. Then the plane of the heme ring is approximately vertical, and the middle of the exposed heme edge has $\theta \sim 90°$. The figure shows the regions where binding of the Ln$^{3-}$ species can occur. Two prominent binding sites are found; one encompasses K13, and the other is near K25; both are relatively close to the exposed heme edge.

Arean et al.[40] have identified four binding sites for anions (A1−A4) in horse heart ferricytc. In the binding site A1 the charged residues Lys5, 87, and 88 are involved; their average position is ∼(150°, 130°). A2, which is near Lys7, 25, and 27 and His26, is centered around ∼(60°, 250°), and A3 encompasses Lys13, 72, and 79, and its center has the coordinates ∼(100°,160°). Both sites A3 and A2 are situated near the heme crevice. The weak binding site A4 (100°, 0°) lies [40−42] at the "back" of the protein, i.e., opposite to the exposed heme edge, near Phe36 and Ile95, and it involves the charged groups Lys99, 53, and 55. Specific binding sites have been reported for phosphate and carbonate anions.[43,44] Phosphate site I lies very close to the sites A3 and A1, and phosphate site II is located near K25, H26, and K27, a region which overlaps with A2. The binding site for carbonate is centered between the residues K72, K73, K86, and K87, and this region also overlaps with A3 and A1.

Figure 7A shows that the electrostatic energy has a minimum near (140°,160°). This region covers (part of) the sites A1 and A3 and also phosphate site I and the carbonate site. The other minimium at (60°, 260°) can be identified as site A2 and phosphate site II. Thus it seems that our electrostatic potentials for cytc, which are similar to those reported by Tiede et al. [45] and Northrup et al.[15] from numerical solutions of the Poisson−Boltzmann equation taking into account the actual shape of the molecule, correctly predict the strongest binding sites A1−A3. This supports the relevance of the method to predict the binding sites of cytc-550 and of its mutants for which corresponding experimental data are lacking.

For cytc-550 (Figure 7B) two binding sites for anions are predicted: an upper site near (140°, 190°) including Lys14, 16, 10, and 106, and a lower one near (60°, 220°), encompassing Lys99, 31, 34, and 54. The replacement of Lys14 (+1) by the

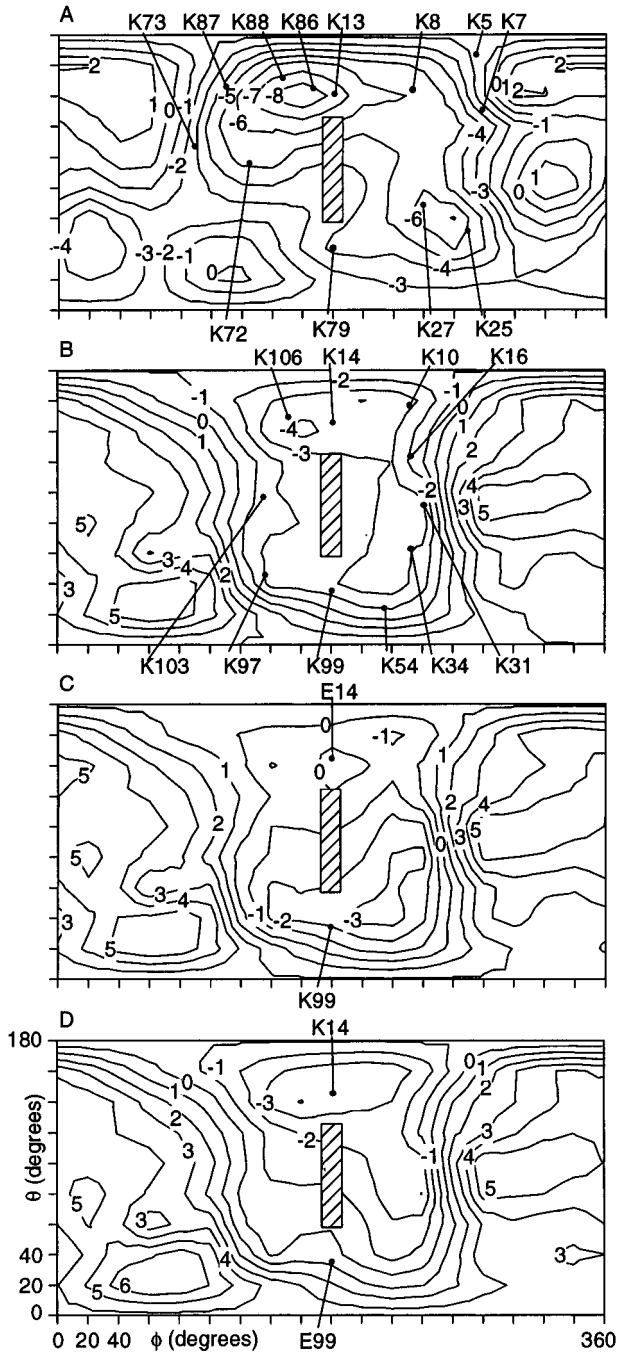


**Figure 7.** Contours maps of the calculated electrostatic potential energy of the −3 Ln complex on the surface of (A) cytc, (B) cytc-550, (C) K14E cytc-550, and (D) K99E cytc-550 in water. Units are $k_BT$ at 293 K. The energies pertain to $I^{1/2} = 0.15$ $M^{1/2}$. The hatched rectangle symbolizes the exposed heme edge; the position of several lysine residues and the mutations are indicated.

negative Glu has a large effect on the potential of the upper site but not on that of the lower site (Figure 7C). Apart from the changes near residue 14, *V* for the mutant is still remarkably similar to that of the wild type. Figure 7D shows the energy calculated for the K99E mutant in which Lys99 has been replaced by a negatively charged Glu. Upon this mutation, the lower binding site is reduced in size whereas the upper binding site is almost unchanged. So it emerges that, at moderate ionic strengths, the electrostatic potential energy is determined mainly by the *local* charge near the protein surface.

We find that in all proteins studied here, the binding of Ln near the exposed heme edge is energetically favorable. For wt cytc-550 the binding energy is smaller than for cytc, which is undoubtedly related to the larger number of negative charges in cytc-550, and the binding area of the protein surface is smaller as well. It is therefore expected that cytc-550 binds anions less strongly (and possibly more specific) than cytc.

An estimate for the order of magnitude of the equilibrium constant for Ln−protein encounter complex formation can be obtained from

$$K = \int_{V_{\text{select}}} g(R,\alpha)\, \mathrm{d}R\, \mathrm{d}a = \int_{V_{\text{select}}} \exp(-q_{\text{Ln}}V/k_BT)\, \mathrm{d}R\, \mathrm{d}\alpha \quad (14)$$

where $V_{\text{select}}$ is such that for a Ln species inside this volume the protein−Ln pair satisfies the criterion for being called a complex. In evaluating *K* we have, rather arbitrarily, used as a criterion that the binding energy should be $\leq -k_BT$. For $I^{1/2} = 0.15$ $M^{1/2}$ we get the results $3 \times 10^3$ $M^{-1}$ (cytc), $2 \times 10^2$ $M^{-1}$ (wt cytc-550), and $1 \times 10^2$ $M^{-1}$ (K14E and K99E cytc-550).

## Discussion

In the results section we have presented experimental data on the enantioselectivity in the quenching of the luminescence of Ln complexes by the ferriproteins. Occasionally these data were obtained from different techniques (analysis of emission decay, $g_{\text{lum}}{}^{\text{cw}}$, and $g_{\text{lum}}(t)$) and yield results that are, as they should be, equal to each other within experimental error. This consistency shows that the two quenching reactions are genuinely diastereomeric ones, and it supports the relevance of the adopted kinetic scheme.

The substantial magnitudes of $E_q$ imply that the transition states for the quenching reactions correspond to geometries where Ln* and protein are in close contact because, generally, large enantioselectivities are due to short-range interactions ("lock-and-key" relationship). If the energy transfer between Ln* and the heme chromophore is a long-range effect, the lock-and-key complex might involve binding of Ln* at any place on the protein surface. If it is short range, the transition state for energy transfer would involve a geometry in which Ln* is close to the exposed heme edge. To get some further insight into this matter we have tried to model the energy transfer process (that is, step 2 in kinetic scheme, $k_{et}$), but first we discuss the peculiar dependence of the quenching rate constants on lanthanide concentration and on ionic strength. The latter aspects relate to the electrostatic binding energy of the Ln* and Q species in the encounter complex (that is, step 1 in kinetic scheme, *K*). Subsequently, we discuss the effects of mutation of the protein and variation of the Ln ion on the enantioselectivity, and finally molecular geometries will be sought that can account for the observed effects.

**[Ln]-Dependence.** The decrease of $k_q$ with increasing [Ln] at constant ionic strength is not unprecedented. With the system Tb/Ru(tris-phenanthroline)$_3^{2+}$, similar effects were ascribed to a reduction of the free quencher concentration due to formation of (inactive) ground state complexes of Ln and quencher molecules.[10] In the presence of static association, the concentration of free quencher molecules, [Q], is given by

$$[\mathrm{Q}] = [\mathrm{Q}]_0 - [\Delta\text{-LnQ}] - [\Lambda\text{-LnQ}] = [\mathrm{Q}]_0 - (K'^{\Delta}[\Delta\text{-Ln}] + K'^{\Lambda}[\Lambda\text{-Ln}])[\mathrm{Q}] = [\mathrm{Q}]_0(1 + K'[\mathrm{Ln}])^{-1} \quad (15)$$

In (15) $K'$ stands for the average of $K'^{\Delta}$ and $K'^{\Lambda}$, where $K'^{\sigma}$ ($= k'_{\mathrm{d}}{}^{\sigma}/k'_{-\mathrm{d}}{}^{\sigma}$) is the equilibrium constant for formation of ground state $\sigma$-LnQ complexes (see Scheme 1). As mentioned, $[\mathrm{Ln}]_0 \gg [\mathrm{Q}]_0$ and therefore $[\mathrm{Ln}] \approx [\mathrm{Ln}]_0$, and so we have instead of (11)

$$k = k_0 + k_{et} K[Q]_0(1 + K'[Ln]_0)^{-1} \quad (16)$$

This formula shows that the decay constant $k$ still is proportional to the total quencher concentration $[Q]_0$, but that—in contrast to (11)—the quenching rate constant $k_q$ which is equal to $k_{et}K(1 + K'[Ln]_0)^{-1}$, depends on the lanthanide concentration: ground state Ln acts as a competitive inhibitor of cytc in the quenching process.

It is important to note that the enantioselectivity is not influenced by the lowering of effective quencher concentration because both diastereomeric rate constants are lowered by the same factor $(1 + K'[Ln]_0)$ which cancels when taking the ratio $k_q^{\Delta}/k_q^{\Lambda}$ or $(k_q^{\Delta} - k_q^{\Lambda})/(k_q^{\Delta}+k_q^{\Lambda})$.

Using (17), which is derived from (16), the magnitude of $K'$ can be estimated from the values of the average quenching rate constants at two Ln concentrations but the same values of [Q] and $I$ (denoted by the superscripts high and low).

$$K' = (k_q^{high} - k_q^{low})/(k_q^{low}[Ln]^{low} - k_q^{high}[Ln]^{high}) \quad (17)$$

This yields the following values of $K'$ (at $I^{1/2} = 0.15$ $M^{1/2}$ and $T = 300$ $K$): $7 \times 10^2$ (cytc) and $4 \times 10^2$ $M^{-1}$ (cytc-550). Thus the quenching rate constants for cytc and wt cytc-550 in Table 1 can be corrected for the formation of inactive quencher complexes by multiplying them by 1.7 and 1.4, respectively.

Qualitatively, the observation that the slopes of ln $k_q^{\Delta}$ and ln $k_q^{\Lambda}$ *vs* $I^{1/2}$ with cytc are steeper at lower [Tb] can be explained by appreciating (18). In this equation the right-hand side results in the limit of very high lanthanide concentration.[46] Since the ionic strength dependencies of $K^{\sigma}(I)$ and $K'(I)$ will be very similar, that of $k_q^{\sigma}$ will be reduced at high Tb concentrations. The calculated values for $K'$ ($3 \times 10^3$ $M^{-1}$ for cytc and $2 \times 10^2$ $M^{-1}$ for wt cytc550; see above) are of the same order of magnitude as the experimental values.

$$k_q^{\sigma} = k_{et} K^{\sigma}(I)[Q]_0(1 + K'(I)[Ln]_0)^{-1} \rightarrow k_{et}^{\sigma}(K^{\sigma}(I)/K'(I))([Q_0]/[Ln]_0) \quad (18)$$

**I- Dependence of the Quenching Rate Constants.** Qualitatively, the slope in a ln $k_q^{\sigma}$ *vs* $I^{1/2}$ plot is related to the product of $q_{Ln}$ and the charge of the protein at the quenching site. In cytc the positive charge is mainly located near the exposed heme edge, and cytc-550 also has positive charge there. So the observation that the slope is more negative for cytc than for cytc-550 is consistent with the idea that it is the region around the heme edge which is involved in the quenching.

More detailed, the effect of variation of ionic strength on $k_q$ is given by (19), an equation being obtained from (16) by putting the binding constants $K$ and $K'$ equal to (20). $V(I)$ is calculated for $\phi = 0°$, $\theta = 90°$, $R = 25$ Å (cytc), and $R = 26$ Å (cytc-550), positions which correspond to the exposed heme edge of the proteins.

$$k_q(I) = k_{et} K(I)/(1 + [Ln]_0 K(I)) \quad (19)$$

$$K(I) = c \exp(-q_{Ln}V(I)/k_BT) \quad (20)$$

At this moment we treat $k_{et}$ in (19) as an adjustable parameter, and we choose the constant $c$ in (20) such that $K(I)$ equals the experimental value of $K'$. In (20) the potential of mean force is approximated by $q_{Ln}V$, but this does not imply that we exclude other than electrostatic charge−charge interactions: as long as the other intermolecular interactions do not depend on $I$, their contribution to $K$ can be cast in the parameter $c$. Figures 4 (cytc-550) and 5 (cytc) show how (19) models the $I$-dependence of the quenching rate constants at the two different lanthanide concentrations.

For cytc the calculated electrostatic potential energy is found to be a monotonously decreasing function of $I^{1/2}$. The $k_q$ curve at low [Ln] to which it gives rise (Figure 5) qualitatively reproduces the experimental finding that the slopes in the low and high $I$-regions are different. Also the downward shift of the ln $k_q$ curve for the sample with higher [Ln] is borne out. The latter conclusion holds for cytc-550 as well (Figure 4). With this protein the potential energy shows a maximum at $I^{1/2} = 0.06$ $M^{1/2}$. Although the experimental data for cytc-550 do not cover the complete $I$-range used in the calculations, the $k_q$ curve seems to have a maximum and, in this respect, resembles the calculated curve:[47] the, at first sight, peculiar behavior of the quenching rate constants of cytc-550 at low values of $I$ can be explained with the simple electrostatic model.

The slopes of the ln $k_q$ *vs* $I^{1/2}$ plots in the high $I$-range are about equal for the two mutants and amount to about half of the value for the wt protein (see Table 2). Calculations of the potential energy for $\theta = 90°$, $\phi = 180°$, and $R = 26$ Å are in good agreement with these experimental results. We find that for both proteins the potential energy varies linearly with $I^{1/2}$ in the range $0.15 < I^{1/2} < 0.30$ $M^{1/2}$ with a slope of 3.3 $M^{-1/2}$.

The observation that for all systems investigated the enantioselectivities, $E_q$, and thus the ratios $k_q^{\Lambda}/k_q^{\Delta}$, are practically independent of $I$ implies that the electrostatic potentials for the two diastereomeric complexes, $V^{\Lambda}(I,R^{\Lambda})$ and $V^{\Delta}(I,R^{\Delta})$, are equal (formally they may differ by a constant which is independent of $I$). This indicates that both the effective charge which Λ-Ln* and Δ-Ln* experience at the active site of protein and the donor−acceptor distances are equal, and thus that both Ln* enantiomers transfer their energy at the same distance away from the protein surface and at approximately the same site. Obviously this conclusion holds to the extent that the method has sufficient resolution. In conclusion, the measured ionic strength dependencies are consistent with a model in which both Ln enantiomers bind to the protein near the exposed heme edge before energy transfer occurs.

**Modeling of the Energy Transfer.** The magnitude of the quenching rate constant is given by (13), which allows for the idea that the rate of energy transfer is dependent on the relative distance and orientation of donor and quencher. For the moment we shall disregard chirality as we did in the calculations of $V$.

*Distribution Functions.* Assuming that the dominating interaction between protein and Ln is of electrostatic nature, we calculate the distribution function $g$ mentioned in (13) using $g = \exp(-q_{Ln}V/k_BT)$. As an illustration we have drawn in Figure 8 $g(R,\alpha)$ as a function of $\theta$ at $\phi = 180°$ (i.e., cross section through the heme plane) and $R = 26$ Å (close contact). The peak of $g(R,\alpha)$ at $\theta = 140°$ corresponds to the upper binding site near Lys14, and the peak $\theta = 40°$ to the lower binding site near Lys99. The curve shows that encounter complexes of "types" K14 and K99 are favored by electrostatic interactions, the former most. Since the magnitude of the interactions is relatively small, the encounter complexes are rather loose. Furthermore, Figure 8 nicely illustrates the finding from the calculations that the effect of the mutation is largely local: the replacement of a positive charge at 14 (99) by a negative results mainly in a vanishing of the electrostatic binding potential in the region around 14 (99); the effect at the other binding site is very modest.

*Energy Transfer.* The rate of radiationless intermolecular electronic energy transfer is given by (21) and (22), where $U$ denotes the interaction energy of Ln*Q and LnQ* and where the band shapes of the relevant donor emission spectrum, $f_{em}(\nu)$,

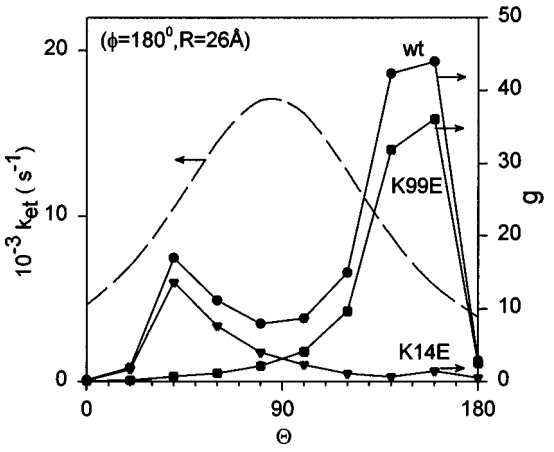


**Figure 8.** Cross sections of the distribution $g(R,\alpha)$ and energy transfer rate $k_{et}(R,\alpha)$ as a function of $\theta$ at $\phi = 180°$ for the cytc-550 proteins. Distribution $g(R,\alpha)$ for wild type (−●−), K14E (−▼−), and K99E (−■−) cytc-550 based upon calculated electrostatic potentials. The dashed curve represents the shape of $k_{et} \sim R_{Ln-Q}^{-6}$.

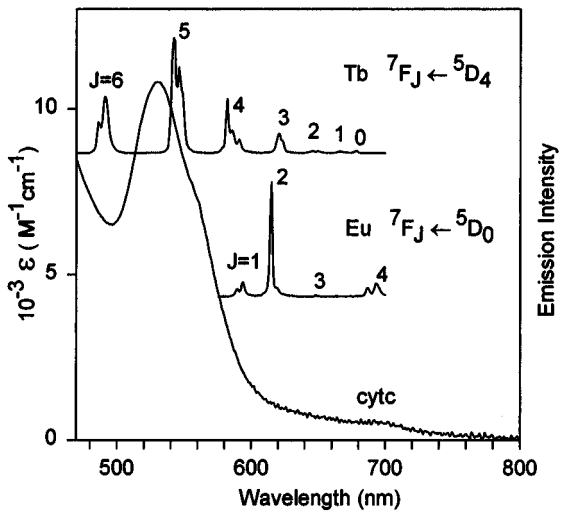


**Figure 9.** Assigned emission bands of Tb and Eu and absorption spectrum of ferricytc from horse heart. The emission spectra have been corrected for the wavelength-dependent response of the detection system.

and acceptor absorption spectrum, $f_{abs}(\nu)$, are normalized to unity.

$$k_{et} = \left(\frac{U}{\hbar}\right)^2 \int f_{abs}(\nu)\, f_{em}(\nu)\, d\nu \qquad (21)$$

$$U = \langle \Psi(Q)\, \Psi(Ln^*)\, |V_{int}|\, \Psi(Q^*)\, \Psi(Ln) \rangle \qquad (22)$$

with

$$\int f_{abs}(\nu)\, d\nu = 1 \text{ and } \int f_{ems}(\nu)\, d\nu = 1$$

The spectral overlap integral in (21) reflects the fact that the energy transfer is isoenergetic and restricts the number of states which can give rise to energy transfer. If we neglect exchange terms, $U$ describes the electrostatic interaction between the charge densities in the relevant transitions of donor, $\Psi(Ln^*)$ $\Psi(Ln)$, and acceptor, $\Psi(Q)$ $\Psi(Q^*)$. We here consider the case that the dominating contributions to $U$ arise from electric dipole−dipole interaction: Foerster-type energy transfer (see (23)). Its value then can be estimated fairly easily from the magnitudes of the transition dipole moments $\mu_{Ln}$ and $\mu_Q$, i.e., the dipole strengths of the relevant spectral transitions, and the distance $R_{Ln-Q}$ between donor (Ln atom) and acceptor (Fe atom in heme). We discuss the isotropic case where the orientation factor $\kappa^2$ equals $^2/_3$.

$$U = \frac{\kappa |\mu_{Ln}||\mu_Q|}{R_{Ln-Q}^{\ 3}} \qquad (23)$$

Figure 9 shows the emission spectra of Tb- and Eu$(DPA)_3^{3-}$ along with the long-wavelength part of the absorption spectrum of horse heart Fe(III)cytc which is due to the heme chromophore ($\sim C_{2v}$ symmetry). The absorptions at ∼520 and ∼560 nm (the $\alpha$ and $\beta$ bands, $\epsilon_{max}$ of the order $10^4$ $M^{-1}$ $cm^{-1}$) are essentially in-plane $(x,y)$ polarized $\pi-\pi^*$ transitions of the porphyrin system. The band at 695 nm ($\epsilon_{max} \sim 1 \times 10^3$ $M^{-1}$ $cm^{-1}$) is currently assigned to a $z$-polarized porphyrin → Fe(III) charge transfer transition.[37] The absorption spectra of the other proteins are very similar. Upon integrating the absorption bands, we get the following values of $\mu_Q$ of the $\alpha,\beta$ band system: 3.6 D (cytc), 3.9 D (cytc-550); for the 700 nm band $\mu_Q$ equals 0.8 D (cytc), 1 D (cytc-550).

Several emission bands of Tb* ($^7F_{6,5,...,0} \leftarrow {}^5D_4$) and Eu* ($^7F_{1,2,4} \leftarrow {}^5D_0$) overlap the absorption spectrum of cytc and thus may be involved in the energy transfer (Figure 9). We assume that the lion's share of the emission intensity is due to electric dipole intensity.[48] From the unquenched luminescence decay constants ($k_0 = 472$ $s^{-1}$ for Tb and 622 $s^{-1}$ for Eu) and estimates for the luminescence quantum yields (0.5 and 0.3), we find the radiative lifetimes and from these the total emission transition dipole moments $\mu_{Ln}$ and that in the individual transitions $\mu_{Ln,i}$. The result is $\mu_{Tb,i} = 3.8$, 5.8, 3.5, 2.2, 1, 1, and $1 \times 10^{-3}$ D for $i = 6$, 5,...,0 in Tb($^7F_i \leftarrow {}^5D_4$) and $\mu_{Eu,i} = 3.5$, 7.1, and $4.2 \times 10^{-3}$ D for the Eu($^7F_i \leftarrow {}^5D_0$) ($i = 1$, 2, 4) transitions.

Figure 8 shows, for cytc-550/Tb, $k_{et}$ as a function of $\theta$ with $\phi$ fixed at 180° and $R$ at 26 Å (i.e., contact between protein and Ln). From the calculations it emerges that $k_{et}$ is a relatively broad function of $\theta$ and $\phi$; energy transfer can occur practically over the entire hemisphere. At contact distance of the donor and quencher spheres and at larger separations, $k_{et}$ is a slowly decaying function of the distance between the Fe and Ln atoms; see (21) and (23). To illustrate this: for cytc-550 $k_{et}$ equals $1.7 \times 10^4$ $s^{-1}$ at contact and $0.7 \times 10^4$ $s^{-1}$ at 5 Å separation between the species. At smaller donor−quencher distances (which are not feasible within our simple model), the value of the derivative of $k_{et}$ with respect to $R$ is much larger. The distribution $g(R,\alpha)$ is broad as well, as a function of $\theta$ (Figure 8) and $\phi$ but also as a function of $R$ (at contact $g = 13$, at 5 Å separation $g = 6$). Consequently the integrand in (13), i.e., the product $g(R,\alpha)$ $k_{et}(R,\alpha)$, is not peaked at a certain position but is rather delocalized. Thus in our model, a relatively large volume around the protein, centered around the exposed heme edge, is involved in the energy transfer step. For cytc a similar conclusion is reached.

From the $\mu_{Ln,i}$ and $\mu_Q$ data, $k_{et}$ can be easily calculated by applying (21) to each of the lanthanide transitions and adding up. Subsequently, using (13), the values of $k_q$ are found to be $1.5 \times 10^7$ (cytc), $1.0 \times 10^6$ (wt cytc-550), and $0.5 \times 10^6$ $M^{-1}$ $s^{-1}$ (cytc-550 K14E and K99E); all values pertain to Tb and $I^{1/2} = 0.15$ $M^{1/2}$. For the case of Eu, the quenching rate constants are calculated to be roughly four times smaller.

*Conclusion.* Compared to the experimental data, these rates are 1 (cytc) and 2 orders of magnitude (cytc-550 proteins) too low. Interestingly, the relative magnitudes of the quenching rates of the wild type cytc-550 and its mutants are predicted more accurately. Next to the underrating of the $k_q$-values, there is a second point where our model does not reproduce the

experimental findings. The large enantioselectivities we observe imply that energy transfer takes place when the protein and Ln* species are in close contact. This means that $g(R,\alpha)\ k_{et}(R,\alpha)$ should be more strongly peaked near the protein surface.

Obviously our model is primitive. First we have neglected other than electrostatic interactions between the Ln and protein species, such as van der Waals interactions and hydrogen bonding which are of short-range type and will increase the height of the distribution function close to the protein surface and at particular values of α. Their inclusion would result in the energy transfer area being more localized close to the protein surface. Secondly, the representation of the protein by a sphere is a serious simplification, particularly in the neighborhood of the exposed heme edge. According to the X-ray and NMR structures of the proteins, Ln−Fe distances shorter than the adopted minimum values of 20 Å (cytc) and 21 Å (cytc-550 proteins) must be possible. The distance from the Fe atom to the carbon atom of the CBC methyl group, which is the most solvent exposed part of the heme ring,[27] amounts to 7 Å. The mean radius of the luminophore, which resembles an oblate spheroid with a polar radius of 2.5 Å and an equatorial one of 7 Å, is 5 Å (see Figure 6). Thus distances between the dipoles as short as 13−15 Å are feasible—without the need for the protein to change its shape. Particularly such close configurations are likely to make an important contribution to the total quenching rate. It is therefore probable that a substantial part of the energy transfer occurs in a region of the exposed heme edge which is more confined than assumed so far. The conclusion that energy transfer requires intimate contact between Ln* and the solvent-exposed heme edge is not invalidated by our reasoning being based on electric dipole−dipole interactions only. Electric dipole−multipole and, particularly, exchange interactions have even a shorter range, and their contributions to $k_{et}$ are expected to be important at small donor−acceptor separations only.

**Difference in Enantioselectivity of Tb and Eu.** In the case of cytc we observe large differences in the enantioselectivity for Tb and Eu; with the other proteins they are much smaller and not clearly beyond the experimental error. The result with cytc is intriguing because $Ln(DPA)_3^{3-}$ complexes have the same, or very nearly so, stereochemical structure along the lanthanide series.[49−51] The wave functions of the electronically excited states of Tb and Eu differ, but they both are based on f−f configurations which involve inner shell orbitals of the central lanthanide atom. To a good approximation many properties will therefore be almost identical for the various $Ln(DPA)_3^{3-}$ *and* $Ln^*(DPA)_3^{3-}$ species. These include the rates of the transport steps $k_d$ and $k_{-d}$ and the bonding in the encounter complex (*K* and *K*′); in terms of (13) the distribution functions $g^\sigma$ are identical for Tb and Eu. However, the function $k_{et}$, involving electronic wave functions, is different for Tb and Eu. Possible explanations for the incongruous $E_q$ values relate to a different $R,\alpha$-dependence of $k_{et}$, to a varying amount of diffusion control in both quenching reactions, or, conceivably, to a different mechanism (energy *vs* electron transfer). We address these three possibilities in reverse order.

Assuming that electron transfer would involve the Fe(III)−Fe(II)cytochrome redox couple, it follows that electron transfer is very unlikely for Eu, since the rare earth ion is already in its highest known oxidation state. Tb(IV) is known, but highly unstable (redox potential for Tb(III)−Tb(IV): +3 V[52]). When we take into account the excitation energy the redox potential Tb*(III)−Tb(IV) becomes about +0.5 V, and electron transfer cannot be excluded on the basis of these data because the potential for the ferro−ferricytochrome couple is +0.260 V for cytc[37] and +0.255 V for cytc-550.[20] Direct experimental evidence for energy transfer is lacking since Fe(III) porphyrins do not fluoresce at room temperature. We find, however, that also Fe(II)cytc quenches Tb and Eu luminescence with rate constants of the same order of magnitude as found with the oxidized protein. We also find that Tb* is efficiently quenched by (free base) tetrakis(4-*N*-methylpyridyl)porphine, a process which gives rise to delayed luminescence from the porphine.[53] Lastly, during our quenching experiments no buildup of reduced cytc could be detected. Altogether this leads us to the judgment that quenching via electron transfer is very unlikely.

The higher $k_q$ values with Tb imply that here the quenching reaction is closer to the diffusion limit than with Eu. Chiral discrimination in a reaction where diffusion is the rate-limiting step is expected to be small when an achiral solvent is used. In fact, it has been proposed that the $E_q \rightarrow 0$ criterion may be used to establish whether a reaction is diffusion controlled,[9,10] but this may not hold if a very specific, close-contact, encounter complex has to be formed.

We also have measured the quenching of $Dy(DPA)_3^{3-}$ luminescence by cytc in $D_2O$ (in the deuterated solvent the luminescence yield and lifetime are larger). It is found that the average quenching rate is ∼1.6 times faster than for Tb while $E_q$ is reduced to $+0.15 \pm 0.01$ (same conditions as in Table 1). The experiment provides an absolute lower bound for the diffusion rate: $k_d \geq 5 \times 10^8\ M^{-1}\ s^{-1}$ (*viz.* $k_q^{\Delta}$, after correction for effective quencher concentration). This shows that in the quenching reaction of cytc/Eu there is no substantial amount of diffusion control, so the measured enantioselectivity approaches the intrinsic $E_q$ value. On the assumption that the latter value is equal for Eu, Tb, and Dy and that $k_d^{\Delta} = k_d^{\Lambda}$, we find from a fit of the quenching rate constants of the six diastereomeric reactions according to (12) that the observed $E_q$ data can be reproduced with $k_d = (7 \pm 1) \times 10^8\ M^{-1}\ s^{-1}$ and the intrinsic value of $E_q$ equal to $0.54 \pm 0.05$.

On the other hand, the data from Figure 5 provide an argument against the reaction with Tb being to a large extent diffusion influenced. The variation of $k_q$ of Tb/cytc with ionic strength covers a dynamic range of no less than 30 in which the value of $E_q$ does not vary at all. Yet one anticipates that $k_{-d}/k_{et}$ increases when *I* is raised and thus that $E_q$ grows in the case of appreciable diffusion control. In fact a change in $k_{-d}$ with *I* by a factor of 2 would already lead to an observable change in $E_q$. Moreover, Figure 5 shows that the shape of $k_q(I)$ is well described by that of $K(I)$.

If the actual energy transfer step is rate limiting, differences in $E_q$ can be brought about by a different distance and/or orientation dependence of $k_{et}$ for Tb and Eu. We insert (13) in (3) to obtain the left-hand side of (24). For the sake of argument

$$E_q = \frac{\int (g^{\Delta} k_{et}^{\Delta} - g^{\Lambda} k_{et}^{\Lambda}) \mathrm{d}R\ \mathrm{d}\alpha}{\int (g^{\Delta} k_{et}^{\Delta} + g^{\Lambda} k_{et}^{\Lambda})\ \mathrm{d}R\ \mathrm{d}\alpha} \cong \frac{\int k_{et} (g^{\Delta} - g^{\Lambda}) \mathrm{d}R\ \mathrm{d}\alpha}{\int k_{et} (g^{\Delta} + g^{\Lambda})\ \mathrm{d}R\ \mathrm{d}\alpha} \tag{24}$$

we assume that the functions $k_{et}^{\Delta}$ and $k_{et}^{\Lambda}$ are about equal. Then we get the right-hand side of (24) which shows that, if the dependence of $k_{et}$ on distance (and/or orientation) with Tb differs from that with Eu, unlike $E_q$ values may result because different parts in space of the varying $(g^{\Delta} - g^{\Lambda})/(g^{\Delta} + g^{\Lambda})$ function are probed by the energy transfer. Obviously the same conclusion is reached if we drop the assumption $k_{et}^{\Delta} \approx k_{et}^{\Lambda}$. In more detail: with Eu the electric dipole−dipole interactions will, at the same donor−quencher distance, be weaker because of the smaller spectral overlap as compared to Tb. Consequently, at contact between Ln* and heme, the shorter-range multipole−

electric dipole and/or electron exchange interactions can play a more important role than with Tb. This results in the function $k_{et}(R)$ falling off more steeply. Accordingly, in the case of Eu the energy transfer occurs at a smaller average distance (i.e., the value of $R$ where the integrand in (13) is peaked) than in the system with Tb. This not only can explain that the $E_q$ values are different, but it also makes plausible that Eu has the larger enantioselectivity because a smaller average distance likely imposes more stringent lock-and-key fitting requirements on the geometry of the transition state.

In conclusion, as yet we cannot assess whether the discrepant $E_q$ values of Tb/cytc and Eu/cytc are due to admixture of diffusion control or to different effective energy-transfer geometries. The reactions of cytc−Tb are possibly diffusion influenced, while those of cytc−Eu are not. On the basis of the $k_q$ and $E_q$ values, there is no indication for diffusion control in the reactions with cytc-550.

**Further Specification of the Quenching Site in the cytc-550 Proteins.** Replacement of a positively charged lysine residue by a negatively charged glutamate at either position 14 or at 99 (i) reduces the quenching rate by approximately a factor of 3 and (ii) lessens the slopes in the ln $k_q^{\sigma}$ *vs* $I^{1/2}$ plots to ∼50% (see Table 2). (iii) The value of $E_q$ is not affected by the first mutation but is about halved by the second one. We take these observations as an indication that Lys14 and Lys99 participate in the electrostatic stabilization of the Ln−protein complex which gives rise to energy transfer (there are no signs for mutation-induced conformational changes[22,54]). For this participation one may envisage two limiting situations: we deal with two quenching sites (one near K14 and the other near K99 with comparable quenching capacities) or with a single quenching site located in between Lys14 and 99.

In the case of two distinct binding sites, the overall enantioselectivity, $E_q^{tot}$, is expected to be an average of the $E_q$ values for the individual sites:

$$E_q^{tot} = \left(\frac{k_{q,14}^{av}}{k_{q,14}^{av} + k_{q,99}^{av}}\right)E_{q,14} + \left(\frac{k_{q,99}^{av}}{k_{q,14}^{av} + k_{q,99}^{av}}\right)E_{q,99} \quad (25)$$

Here $k_{q,14}^{av}$ denotes the average rate constant for quenching at the site near residue 14 and $k_{q,99}^{av}$ denotes that near 99. The mutation of Lys14 → Glu leads to a reduced binding of the Ln complex on site 14 and thus to a lower value of $k_{q,14}^{av}$, but $k_{q,99}^{av}$ is expected to be only slightly influenced by mutation near 14. Consequently the weighting factor $k_{q,14}^{av}/(k_{q,14}^{av} + k_{q,99}^{av})$ will decrease and $k_{q,99}^{av}/(k_{q,14}^{av} + k_{q,99}^{av})$ will increase as compared to the situation with the wild type protein. From the irregularity of the protein surface we expect that $E_{q,14}$ differs from $E_{q,99}$ ; in addition the mutation may affect the magnitude of the enantioselectivities as well. Altogether we expect a change in enantioselectivity upon mutation of K14, but experimentally no such change is observed. So we propose one quenching site, closer to K99 than to K14.

**Molecular Modeling Results.** Using the molecular modeling program Sybyl 6.1,[55] we have searched for low-energy conformations of the diastereomeric Ln/cytc-550 pairs, i.e., ground state binding sites. Guided by the experimental evidence for the involvement of Lys99 in the quenching process, we have taken into account only the region of the protein around this residue (i.e., the front surface of the lower half of the protein as drawn in Figure 6). The conformation of the protein was derived from a crystal structure[31] (see above) and that of the luminophore from the X-ray structure of an $Eu(DPA)_3^{3-}$ complex.[50] The charges of the individual atoms in the protein are calculated by Sybyl; in the lanthanide complex we assigned a +3 charge to the central Eu ion, while the 2− charge of each DPA ligand was calculated to be practically localized on the four carboxylate oxygen atoms.

First the intermolecular geometry was optimized using frozen conformations of Ln and protein. Using starting configurations where the closest part of Ln is situated some 3−4 Å in front of Lys99, we always find low-energy configurations involving hydrogen bonding between the carboxylate oxygen of a DPA ligand and the ϵ-amino group of Lys99. Many of these configurations are rather loose (no close contacts except for the hydrogen bond) and correspond to local energy minima in intermolecular configuration space. Considerably lower minima are found when docking the second DPA ring into the small cavity in the protein surface which is located between Phe53 and Lys54. The favorable van der Waals interactions probably also involve stacking interaction between the DPA ligand and the aromatic ring of Phe53 in the hydrophobic cavity.

Subsequently we fixed the docked $Eu(DPA)_3^{3-}$ in such orientations and allowed for rotations around single bonds in the Lys99, Phe53, and Lys54 side chains. It appears that the ϵ-amino group and amide proton of Lys54 also form hydrogen bonds with the carboxylate oxygens of the DPA ligands. In this procedure the structure of the protein itself remains largely unchanged; the hydrogen bond between Lys99 and the carbonyl of Lys54, which is present in the crystal structure, remains intact. A typical result for Λ-Ln (there is a number of closely related configurations of about the same energy) of the energy minimization is shown in Figure 10 (top). In view of the incomplete search in intermolecular configuration space, possibly other minima exist. However, in the region of the protein around Lys99, the structure of Figure 10 (and closely related ones) is likely to be the energy minimum, representing an occupied binding site of the protein.

It appears that the structure predicted for the Δ-Ln/cytc-550 complex (Figure 10, bottom) is very similar to that of the diastereomeric complex (Figure 10, top) as far as binding of the upper right DPA ligand to the protein is concerned (interaction with Phe53, hydrogen bonding to Lys54 and 99). The position of the other two aromatic ligands is clearly different in both structures. For precisely the configurations depicted in Figure 10, the Δ-Ln diastereomeric complex appears to be the most stable one, but there are closely related pairs of diastereomers where the order is reversed. To forecast the enantioselectivity of the binding one should calculate the Boltzmann distributions of the two diastereomeric complexes, i.e., the distribution functions $g^{\sigma}(R,\alpha)$.

The neglect of solvent molecules and counterions leads to a serious overestimation of the electrostatic interaction energy; probably the short-range interactions are affected less severely. We find that binding of Ln in the same cavity occurs when in the energy minimalization electrostatic interactions are deliberately neglected (realized by putting the charges on Ln and DPA equal to zero). This indicates that the configurations of Figure 10 do not result from overrating the electrostatic binding energy.

As yet we regard the configurations in Figure 10 merely as a working model to study the molecular basis of the quenching reactions. If we assume that the quenching site resembles the binding site, as is suggested by the small temperature effect on the rate of our quenching reactions, the model accommodates the present (limited) experimental knowledge about the energy transfer geometry: binding of Ln close to the heme ring, the importance of Lys99, and the involvement of relatively strong van der Waals interactions and hydrogen bonding between Ln and protein, providing an intimate lock-and-key relationship.

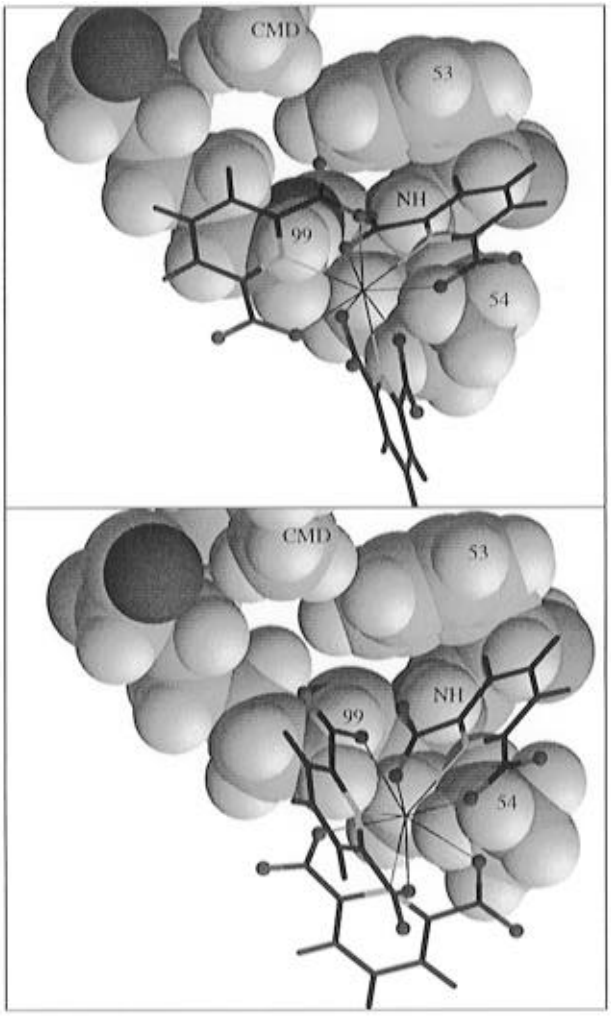


**Figure 10.** Minimal energy conformations of the diastereomeric complexes between cytc-550 and Λ-Eu(DPA)$_3^{3-}$ (top) and Δ-Eu(DPA)$_3^{3-}$ (bottom). The carboxylate oxygens of the DPA ligands hydrogen bind to the ϵ-amino groups of Lys54 and Lys99 and to the amide proton of Lys54 (indicated as NH). There is a stacking interaction between a DPA ring and Phe53. Apart from the CMD methyl group of the heme, the remainder of the protein (see Figure 6) is not shown.

On the other hand, we anticipate that in the configurations of Figure 10 the role of Lys14 in governing the magnitude and ion-strength dependence of the quenching rates may be underexposed.

## Conclusion

We present evidence that the dynamic quenching of the Ln luminescence by cytc and cytc-550 proteins is due to electronic energy transfer which occurs near the exposed heme edge. The calculated electrostatic potentials of the proteins give a first indication where binding of Ln* occurs; for −3 ions a relatively broad and shallow potential well around the exposed heme edge is calculated. The potentials also account qualitatively for the observed ionic strength dependencies of $k_q$. At small distance from the protein surface, short-range interactions will contribute to the intermolecular potential, and they can give rise to localized, and enantioselective, binding sites. In the cytc-550 proteins both Lys99 and Lys14 are involved in the binding, probably the former most. Via molecular modeling a feasible site is obtained for cytc-550; it shows specific binding involving several hydrogen bonds and electrostatic and steric interactions, and it clearly discriminates between the Λ- and Δ-Ln species. These diastereomeric Ln/cytc-550 complexes are tentative and should be tested further, e.g., by studying additional cytc-550 mutants or, making use of the paramagnetism of most Ln(III) ions, by NMR experiments.

Variation of the central Ln ion of the luminophore has a considerable effect on the enantioselectivity in the quenching by cytc, while this is not the case for cytc-550. We have suggested two possible explanations for this effect. However, at this moment we are not able to chose between these; a major question which remains open is the effect of diffusional motion on the enantioselectivity with cytc.

Our study shows that enantioselective luminescence quenching using chiral lanthanide complexes is a promising tool in probing the electrostatic potential and the structure of the active site of metalloproteins. The technique is relatively fast and requires only small amounts of protein. It is not restricted to Fe(III)-cytc proteins as it, for instance, also works for the Fe(II) species.

Interestingly several electron transfer reactions of cytc have been reported to occur at the exposed heme edge as well. These include redox reactions with small inorganic complexes[56−58] and also physiologically important charge transfer processes.[59,60] Pelletier and Kraut[61] have proposed that the pyrrole C ring of the heme (i.e., the pyrrole which in cytc is close to K13) is involved in (biological) electron transfer reactions. Interestingly, our results for cytc-550 point to the area around the pyrrole D ring (close to K99) as the energy transfer site. One may anticipate that the (enantioselective) quenching of the luminescence from chiral lanthanide chelates is not merely an alternative, but also a complementary, way to study the active site of metalloproteins. Being based on energy transfer, which presumably has another distance and orientation dependence than does electron transfer, the method may well probe another part of the protein's structure. A specific application is the following. Electron transfer reactions between inorganic substrates and a protein occasionally are found to be sensitive to pH, an effect which can reside in the binding or in the electron transfer step in the encounter complex.[62,63] In such cases the comparison with an energy transfer reaction may be informative because the spectroscopic properties of the metal site of the protein, and therefore the energy transfer rate ($k_{et}$), may well be less susceptible to pH than the redox potential.

## References and Notes

(1) Metcalf, D. H.; Snyder, S. W.; Wu, S.; Hilmes, G. L.; Riehl, J. P.; Richardson, F. S. *J. Am. Chem. Soc.* **1989**, *111*, 3082.
(2) Metcalf, D. H.; Snyder, S. W.; Demas, J. N.; Richardson, F. S. *J. Am. Chem. Soc.* **1990**, *112*, 5681.
(3) Metcalf, D. H.; Stewart, J. M. McD.; Snyder, S. W.; Grisham, C. M.; Richardson, F. S. *Inorg. Chem.* **1992**, *31*, 2445.
(4) Metcalf, D. H.; Bolender, J. P.; Driver, M. S.; Richardson, F. S. *J. Phys. Chem.* **1993**, *97*, 553.
(5) Bolender, J. P.; Metcalf, D. H.; Richardson, F. S. *Chem. Phys. Lett.* **1993**, *213*, 131.
(6) Richardson, F. S.; Metcalf, D. H.; Glover, D. P. *J. Phys. Chem.* **1991**, *95*, 6249.
(7) Glover, D. P.; Metcalf, D. H.; Bolender, J. P.; Richardson, F. S. *Chem. Phys.* **1995**, *198*, 207.
(8) Rexwinkel, R. B.; Meskers, S. C. J.; Riehl, J. P.; Dekkers, H. P. J. M. *J. Phys.Chem.* **1992**, *96*, 1112.
(9) Rexwinkel, R. B.; Meskers, S. C. J.; Dekkers, H. P. J. M.; Riehl, J. P. *J. Phys. Chem.* **1992**, *96*, 5725.
(10) Rexwinkel, R. B.; Meskers, S. C. J.; Riehl, J. P.; Dekkers, H. P. J. M. *J. Phys. Chem.* **1993**, *97*, 3875.
(11) Rexwinkel, R. B.; Meskers, S. C. J. ; Dekkers, H. P. J. M.; Riehl, J. P. *J. Phys. Chem.* **1993**, *97*, 13519.
(12) Metcalf, D. H.; Snyder, S. W.; Demas, J. N.; Richardson, F. S. *J. Am. Chem. Soc.* **1990**, *112*, 469.
(13) Wensel, T. G.; Meares, C. F. *Biochemistry* **1983**, *22*, 6247.
(14) Yeh, S. M.; Meares, C. F. *Biochemistry* **1980**, *19*, 5057.
(15) Northrup, S. H.; Wensel, T. G.; Meares, C. F.; Wendolski, J. J.; Matthews, J. B. *Proc. Natl. Acad. Sci. U.S.A.* **1990**, *87*, 9503.

(16) Pladziewicz, J. R.; Accola, M. A.; Osvath, P.; Sargeson, A. M. *Inorg. Chem.* **1993**, *32*, 2525.
(17) Bernauer, K. *Metal ions in Biological Systems*; Sigel, H. Sigel, A., Eds.; Marcel Dekker Inc.: New York, 1991; Vol. 27, p 265.
(18) Rexwinkel, R. B. Ph.D. Thesis, Leiden University, 1993.
(19) McQuarrie, D. A. *Statistical Mechanics*; Harper & Row: New York, 1976.
(20) Lommen, A.; Ratsma, A.; Bijlsma, N.; Canters, G. W.; Van Wielink, J. E.; Frank, J.; Van Beeumen, J. *Eur. J. Biochem.* **1990**, *192*, 653.
(21) Ubbink, M.; Van Beeumen, J.; Canters, G. W. *J. Bacteriol.* **1992**, *174*, 3707.
(22) Ubbink, M.; Canters, G. W. *Biochemistry* **1993**, *32*, 13893.
(23) Ubbink, M.; Warmerdam, G. C. M.; Campos, A. P.; Teixeira, M.; Canters, G. W. *FEBS Lett.* **1994**, *351*, 100.
(24) Van Gelder, F.; Slater, E. C. *Biochim. Biophys. Acta* **1962**, *58*, 593.
(25) Rexwinkel, R. B.; Schakel, P.; Meskers, S. C. J.; Dekkers, H. P. J. M. *Appl. Spectrosc*. **1993**, *47*, 731.
(26) Press, W. H.; Flannery, B. P.; Teukolsky, S. A.; Vetterling,W. T. *Numerical Recipes*; Cambridge University Press: Cambridge, U.K., 1986.
(27) Qi, P. X.; Di Stefano, D. L.; Wand, A. J. *Biochemistry* **1994**, *33*, 6408.
(28) Bernstein, F. C.; Koetzle, T. F.; Williams, G. J. B.; Meyer, E. F., Jr.; Brice, M. D.; Rodgers, J. R.; Kennard, O.; Shimanouchi, T.; Tasumi, M. *J. Mol. Biol.* **1977**, *112*, 535.
(29) Abola, E. E.; Bernstein, F. C.; Bryant, S. H.; Koetzle, T. F.; Weng, J. *Crystallographic Databases-Information Content, Software Systems, Scientific Applications*; Allen, F. H., Bergerhoff, G. Sievers, R., Eds.; Data Commission of the International Union of Crystallography: Bonn/Cambridge/ Chester, 1987.
(30) Wherland, S.; Gray, H. B. *Proc. Natl. Acad. Sci. U.S.A.* **1976**, *73*, 2950.
(31) Benning, M. M.; Meyer, T. E.; Holden, H. M. *Arch. Biochem. Biophys.* **1994**, *310*, 460.
(32) Timkovich, R.; Dickerson, R. E. *J. Biol. Chem.* **1976**, *251*, 4033.
(33) Hilmes, G. L.; Riehl, J. P. *Inorg. Chem.* **1986**, *25*, 2617.
(34) Metcalf, D. H.; Richardson, F. S. *J. Alloys Compd.* **1994**, *207*−208, 59.
(35) Pettigrew, G. W.; Moore, G. R. *Cytochromes c. Biological aspects*; Springer Verlag: Berlin,1987.
(36) Moore, G. W.; Pettigrew, G. R. *Cytochromes c. Evolutionairy, Structural and Physiochemical aspects*; Springer Verlag: Berlin,1990.
(37) Theorell, H.; Åkesson, Å. *J. Am. Chem. Soc.* **1941**, *63*, 1804.
(38) Marcus, R. A.; Sutin, N. *Biochim. Biophys. Acta* **1985**, *811*, 265.
(39) (a) Head-Gordon, T.; Brooks, C. L., III. *J. Phys. Chem.* **1987**, *91*, 3342. (b) Head-Gordon, T.; Brooks, C. L., III *J. Phys. Chem.* **1989**, *93*, 490. (c) Although the authors recommend otherwise, we have used the formula they give in ref 39a and not the one which they propose in ref 39b−for several reasons. The formula in ref 39b does not reduce to Coulomb's law in the case of only one charge on the protein, $I = 0$, and $\epsilon_1 = \epsilon_2$. Neither does it reduce to the formula that can be derived for a point dipole. Lastly, proceeding along the lines sketched by Kirkwood[39d] and by ref 39a, one does arrive at the result given in ref 39a, not at that stated in ref 39b. (d) Kirkwood, J. G. *J. Chem. Phys.* **1934**, *2*, 351.
(40) Arean, C. O.; Moore, G. R.; Williams, G.; Williams, R. J. P. *Eur. J. Biochem*. **1988**, *173*, 607.
(41) Eley, C. G. S.; Moore, G. R.; Williams, G.; Williams, R. J. P. *Eur. J. Biochem*. **1982**, *124*, 295.
(42) Williams, G.; Eley, C. G. S.; Moore, G. R.; Robinson, M. N.; Williams, R. J. P. *FEBS Lett.* **1982**, *150*, 293.
(43) Ferguson-Miller, S.; Brautigan, D. L.; Margoliash, E. *J. Biol. Chem.* **1978**, *253*, 149.
(44) Osheroff, N.; Brautigan, D. L.; Margoliash E. *Proc. Natl. Acad. Sci. U.S.A.* **1980**, *77*, 4439.
(45) Tiede, D. M.; Vashista, A.-C.; Gunner, M. R. *Biochemistry* **1993**, *32*, 4515.
(46) When $K'(I)$ is a very steep function of $I$, lowering of I leads to a sharp increase of $K'(I)$ and, for low enough values of $I$, $K'(I)[\mathrm{Ln}]_0 \gg 1$. Also, then the right-hand side of (18) results.
(47) Other observations of such "convex" ln $k$ *vs* $I^{1/2}$ curves include the kinetics of the MADH redox chain.[60] The effect has also been observed for the association of methanol dehydrogenase and cytochrome c551i (Harris, T. K.; Davidson, V. L.; Chen, L.; Mathews, F. S.; Xia, Z. *Biochemistry* **1994**, *33*, 12600) where it was interpreted in terms of Van Leeuwen theory (Van Leeuwen, J.; Mofers, F. J. M.; Veerman E. C. I. *Biochim. Biophys. Acta* **1981**, *635*, 434). Physically our calculated curve can be understood as follows. At very low values of $I$, the negative charges on the other side of the protein also contribute to the potential at the heme side, and their influence tends to repel negative ions at the heme side. At higher $I$, cations from the solution reside near the highly negative charged side, negative charges are shielded, and their influence on the potential near the exposed heme edge diminishes. The potential is more and more determined by the local (positive) charge density. Upon further increase of $I$, also the positive charge is shielded leading to a decrease of $k_q$. It has been concluded from the $I$-dependence of the bandwidths of certain $^1$H NMR signals of cytc-550 that at low $I$ the protein can adopt a conformation with a more open heme crevice.[22] It is conceivable that such conformational freedom contributes to the observed behavior of the quenching rate constants as well. We see no need to invoke a conformational change in the description of the quenching at low ionic strength because the enantioselectivity in the quenching does not change appreciably with $I$.
(48) This does not hold for the band Eu $^7F_1 \leftarrow {}^5D_0$ which has mainly magnetic dipole intensity (ref 34 and Meskers, S. C. J.; Riehl, J. P.; Dekkers, H. P. J. M. *Chem. Phys. Lett.* **1993**, *216*, 241) The Tb $^7F_{5,4,3} \leftarrow {}^5D_4$ transitions may carry a considerable amount of magnetic dipole intensity (Saxe, J. D.; Morley, J. P.; Richardson, F. S. *Mol. Phys.* **1982**, *47*, 407).
(49) Albertsson, J. *Acta Chem. Scand.* **1972**, *26*, 1023.
(50) Structural data for $Eu(DPA)_3^{3-}$ and $Tb(DPA)_3^{3-}$ are available from the Cambridge Structural Database under entries SOPFUY and JEXWOY, respectively, with references to: Shengzhi, H.; Zhenchao, D.; Huizhen, Z.; Qiwang, L. *Xiamen Daxue Xuebao, Ziran Kexueban J. Xiamen Univ., Nat. Sci.)* **1989**, *28*, 279, 514.
(51) Sherry, A. D.; Geraldes, C. F. G. C. *Lanthanide probes in Life, Chemical and Earth Sciences*; Bünzli, J.-C. G., Choppin, G. R., Eds.; Elsevier: Amsterdam, 1989; Chapter 4.
(52) Hart, F. A. *Comprehensive Coordination Chemistry*; Wilkinson, G., Ed.; Pergamon Press: Oxford U.K., 1987; Vol. III, Chapter 39.
(53) Meskers, S. C. J.; Dekkers, H. P. J. M. Unpublished results.
(54) Ubbink, M.; Campos, A. P.; Teixeira, M.; Hunt, N. I.; Hill, H. A. O.; Canters, G. W. *Biochemistry* **1994**, *33*, 10051.
(55) Molecular modeling system SYBYL, Tripos Associates Inc., St. Louis, MO 63177.
(56) Ahmed, A. J.; Millet, F. *J. Biol. Chem.* **1981**, *256*, 1611.
(57) Butler, J.; Davies, D. M.; Sykes, A. G.; Koppenol, W. H.; Osheroff, N.; Margoliash, E. *J. Am. Chem. Soc*. **1981**, *103*, 469.
(58) Butler, J.; Chapman, S. K.; Davies, D. M.; Sykes, A. G.; Speck, S. H.; Osheroff, N.; Margoliash, E. *J. Biol. Chem.* **1983**, *258*, 6400.
(59) Caffrey, M. S.; Bartsch, R. G.; Cusanovich, M. A. *J. Biol. Chem.* **1992**, *267*, 6317.
(60) Ubbink, M.; Hunt, N. I.; Hill, H. A.; Canters, G. W. *Eur. J. Biochem.* **1994**, *222*, 561.
(61) Pelltier, H.; Kraut, J. *Science* **1992**, *258*, 1748.
(62) Segal, M. G.; Sykes, A. G. *J. Am. Chem. Soc.* **1978**, *100*, 4585.
(63) Lappin, A. G.; Segal, M. G.; Weatherburn, D. C.; Sykes, A. G. *J. Am. Chem. Soc*. **1979**, *101*, 2297.

JP961381Z